Formation of stacking faults and their correlation with flux pinning and critical current density in Sm-doped YBa_{2}Cu_{3}O_{7-δ} films

Sung Hun Wee, Eliot D. Specht, Claudia Cantoni, Yuri L. Zuev, Victor Maroni, Winnie Wong-Ng, Guangyao Liu, Timothy J. Haugan, and Amit Goyal

Phys. Rev. B **83**, 224520 — Published 29 June 2011

DOI: 10.1103/PhysRevB.83.224520

Formation of stacking faults and their correlation with flux-pinning and critical current density for Sm-doped $YBa_2Cu_3O_{7-\delta}$ films

Sung Hun Wee[1,*], Eliot D. Specht[1], Claudia Cantoni[1], Yuri L. Zuev[1,2], Victor Maroni[3], Winnie Wong-Ng[4], Guangyao Liu[4], Timothy J. Haugan[5], and Amit Goyal[1,*]

[1]*Materials Science and Technology Division, Oak Ridge National Laboratory, Oak Ridge, Tennessee 37831, USA*

[2]*Department of Physics, University of Tennessee, Knoxville, Tennessee 37996, USA*

[3]*Argonne National Laboratory, Argonne, IL 60439*

[4]*Ceramic Division, National Institute of Science and Technology, Gaithersburg, MD 20899*

[5]*AFRL/RZPG, The Air Force Research Laboratory, Wright-Patterson AFB, OH 45433*

Abstract

A correlation between flux-pinning characteristics and stacking faults (SFs) formed by Sm substitution on Y and Ba sites was found in Sm-doped $YBa_2Cu_3O_{7-\delta}$ (YBCO) films. It was confirmed that 223-type-SFs, $Y_2Ba_2Cu_3O_x$, composed of extra Y and O planes aligned parallel to the *ab*-planes formed via Sm substitution on the Y site and increased in number with increasing Sm doping on the Ba site. The number density of 223 SFs is correlated strongly with the enhancement in *ab*-plane correlated flux-

*Corresponding authors: wees@ornl.gov, goyala@ornl.gov

pinning, resulting in a sharpening of the $H \| ab$ peak in the plot of critical current density versus magnetic field orientation.

PACS: 74.72.-h; 74.78.Na; 74.25.Wx; 84.71.Mn

I. INTRODUCTION

Flux-pinning and critical current density, J_c, for YBCO superconducting films has been remarkably strengthened by the controlled incorporation of nanoscale defects into the films.[1-6] In particular, epitaxial growth of self-organized, non-superconducting nanoscale defects aligned parallel to the *c*-axis of the film has resulted in strongly improved pinning and enhanced J_c, particularly for the case where the magnetic field is also aligned parallel to the c-axis, $H \| c$.[4-6] In addition to the incorporation of nanoscale defects, rare-earth (RE) element substitution in YBCO has been considered a complementary method for synergistic enhancement of flux-pinning. In fact, $REBa_2Cu_3O_{7-\delta}$ (REBCO) superconductors especially those with RE = Nd, Sm, Eu, and Gd have been reported to result in superior superconducting performance including larger T_c, J_c, and irreversibility field, H_{irr}, as compared to un-doped YBCO.[7] It has been argued that small amounts of RE substitution into the Ba site (driven by their similar ionic sizes) create strong pinning centers that are nanoscale low T_c phases, without sacrificing the overall T_c.[7] Synergetic improvement in flux-pinning by incorporation of $BaZrO_3$ (BZO) into REBCO films has also been demonstrated.[8-9] However, fabrication of high quality REBCO films requires modification of growth conditions with typically higher growth temperature and/or lower oxygen partial pressure, or an additional seed layer to achieve 100% *c*-axis oriented films and to suppress excess RE substitution into the Ba site that significantly reduces T_c.[10-12] That is why the successful growth of high quality REBCO films with higher self-field J_c compared to YBCO films is not commonly achieved.

Previous studies have demonstrated that partial RE substitution onto the Y site would be a more effective and practical approach to achieving high J_c films without

changing growth conditions.[13-16] $Y_{1-x}RE_xBCO$ films with RE substitutions in the range of x = 0.1 to 0.5 have been reported to have higher self-field J_c with enhanced in-field performance, as well as a higher T_c even though the samples were deposited at identical growth conditions to the YBCO films. Additional nanoscale imperfections created by local strain fields associated with variations in ionic size between the RE and Y have been considered as a possible origin for such J_c improvement.[13-15] However, there are no reports that clearly identify the types of defects that are dominantly formed and act as major pinning centers when the partial substitution of RE elements is realized.

In this study, we discovered a particular type of defects that originated when Sm was substituted on the Ba site as well as on the Y site in YBCO films and we investigated their correlation to flux-pinning characteristics.

II. EXPERIMENTAL METHODS

$(Y_{0.667}Sm_{0.333+x})Ba_{2-x}Cu_3O_{7-\delta}$ (YSmBCO) films with different x in the range from 0 to 0.15 were grown by pulsed laser deposition (PLD). Selection of RE element and the amount of RE substitution for the parent (x=0) sample for this study was based on the previous study reporting that $(Y_{0.667}Sm_{0.333})Ba_2Cu_3O_{7-\delta}$ had the highest J_c performance among $Y_{1-x}RE_xBCO$ samples with various RE elements and substitution amounts.[15] PLD deposition conditions for the films were identical to those for pure YBCO films.[6,17] The film growth temperature, T_s, was 1063 K and the oxygen partial pressure, $P(O_2)$, was 230 mTorr. All depositions were performed on ion-beam-assisted deposition (IBAD)-MgO templates with a $LaMnO_3$ cap layer that were supplied by Superpower, Inc.[18] A film thickness of ~800 nm was confirmed by cross sectional transmission electron microscopy

(TEM) analysis. After deposition, the samples were *in-situ* annealed at T_s = 773 K and $P(O_2)$ = 500 Torr for 30 min. Ag electrodes were then sputtered onto the films followed by *ex-situ* annealing at 773 K for 1 h in flowing O_2 gas. In-field transport J_c of the samples was measured using the standard four-probe method while applying magnetic fields, after the samples were patterned to a 200 μm-bridge-width by laser scribing. The angular dependence of J_c was measured in the maximum Lorentz force configuration in which the field direction is always perpendicular to the direction of the current. Cross sectional microstructures were characterized by transmission electron microscopy (TEM). TEM cross-section specimens were prepared using the focused-ion beam (FIB) technique. Texture and phase analysis was performed using X-ray diffraction (XRD).

III. EXPERIMENTAL RESULTS AND DISCUSSIONS

XRD results including θ-2θ scans, (006) ω-scans, (113) φ- scans and pole figures indicate that all the YSmBCO samples have excellent cube-on-cube epitaxy with 100% *c*-axis orientation. As summarized in Table 1, the samples have small full-width-half-maximum (FHWM) values of in-plane (Δφ) and out-of-plane (Δω) orientations and sharp cube texture over 95%. However, as shown in Fig. 1(a), the YBCO (006) peak broadens with increasing amounts of Sm substitution. Bragg peak broadening is commonly analyzed using the Williamson-Hall plot[19], where the scaled peak broadening is constant for finite-size and increases linearly with increasing strain. As shown in Fig. 1(b), the broadening is oscillatory, indicating that stacking faults (SFs) are the cause. Hendricks and Teller describe in their Eq. (6) how one can calculate the diffraction pattern for a material consisting of randomly stacked layers of material.[20] In order to determine an

unknown type of stacking fault, we simplify this formula by taking the limit where a fraction $f << 1$ of the layers have thickness d_2, while the remaining fraction $1 - f$ has a thickness d_1. To first order in f, the Bragg reflection of order n has a Lorentzian line shape

$$I(2\theta) \sim [1 + 4(2\theta - 2\theta_0)^2/w^2]^{-2}, \quad (1)$$

where the peak FWHM is given by

$$w = 2f(1-\cos\phi), \quad (2)$$

the peak shift is given by

$$2\theta_0 - 2\theta_1 = f\lambda\sin\phi/2\pi d_1\cos\phi, \quad (3)$$

where $\phi = 4\pi d_2\sin\theta/\lambda$, and θ_1 is the unshifted Bragg angle $\theta_1 = \sin^{-1}(n\lambda/2d_1)$. The nature of the stacking fault is determined by measuring the width and shift of a series of (00*l*) reflections and fitting the values to Eqs. (2) and (3) using f and d_2 as free parameters. As shown in Fig. 1(b), a good fit to both the peak shifts and the peak widths is obtained for a stacking fault with a thickness of 1.43 nm. This corresponds well with the 223 stacking faults observed in YBCO having a thickness of 1.41 nm, consisting of extra planes of Y and O.[21] This is further confirmed by comparing the observed diffraction pattern to a simulated pattern using the complete Hendricks-Teller model, as shown in Fig. 1(c). Figure 1(d) shows the number density of 223 SFs as a function of the amount of Sm substitution estimated by the model. While no SFs for the pure YBCO sample are estimated, the SFs start forming in the case x=0 when only Sm substitution into the Y site should occur and linearly increase with increasing Sm substitution on the Ba site up to a linear density of ~52 μm^{-1} at x=0.15.

Formation of 223 SFs was also visually confirmed by cross-sectional TEM examination of the same YSmBCO samples used for XRD analysis. Figures 2 (a) and (b) show TEM images taken from the samples with Sm substitution on the Y site only (x=0) and on both Y and Ba sites (x=0.15). As denoted by black arrows, 223 SFs aligned along the *ab*-planes of the film are observed in both samples. The x=0.15 sample has a higher number density of SFs than the x=0 sample. This result is consistent with XRD measurements showing an increase in SF density with increasing x. Aberration corrected Z-contrast (where Z=atomic number) scanning transmission electron microscopy (STEM) imaging was also used to identify the atomic structure of 223 SFs as shown in Fig. 2(c), where the lattice image of a 223 SF having extra Y and O planes is shown. Crystal structures corresponding to YBCO and a 223 SF are illustrated in the right side of the figure.

Table 1 summarizes superconducting properties including T_c and J_c at 77 K, self-field for the set of YSmBCO films with different x values. The data for a pure YBCO film prepared under an identical growth condition are also shown for comparison. All of the YSmBCO samples exhibit T_c of 87.4 ~ 88.3 K that are nearly unchanged from the T_c of 87.7 K for pure YBCO. However, there is considerable change in the J_c as a consequence of Sm substitution onto Y and Ba sites. First, the J_c is noticeably improved from 2.8 to 4.0 MA/cm^2 by Sm substitution on the Y sites. The J_c improvement can be ascribed to the formation of an optimal density of 223 SFs in the film. As reported from an earlier study of YBCO films with BZO additions, an optimum BZO doping also increases self-field J_c as well as in-field J_c.[17] However, after an initial enhancement, J_c gradually degrades with additional Sm substitution on the Ba sites. The J_c of the x = 0.05

sample is reduced to ~3.4 MA/cm^2, which is still larger than the J_c for pure YBCO. J_c drops further to 2.2 and 0.8 MA/cm^2, with increasing x from 0.1 to 0.15.

There are two possible reasons for this reduction. First, the J_c can be reduced by the formation of second phases, such as Ba-Cu-O and CuO (or Cu_2O), although no surface particles of these phases were observed. Excess Sm substitution on the Ba site can produce such excess phases which can segregate at grain boundaries and reduce the J_c. Second, excess cation and oxygen disorder effects can develop with increasing Sm substitution on the Ba site and cause a reduction of J_c. In support of the latter cause for the observed J_c decrease, Raman spectroscopy measurements reveal a significant increase in phonon bands corresponding to both cation disorder and oxygen disorder with increasing Sm content, as shown in Fig. 3. This figure shows Raman spectra for YSmBCO films with x=0 (red) and x=0.15 (purple) with intensities normalized to the 330 cm^{-1} YBCO mode, and the difference spectrum (blue dot line) obtained by subtracting the x=0 spectrum from the x=0.15 spectrum. The x=0.15 sample has the much increased phonon modes at 230 cm^{-1} and 560 cm^{-1} that indicate significantly more cation disorder and oxygen disorder than the x=0 sample. As shown in Fig. 4, an analysis of the intensity variations in a Z-contrast STEM image (similar to that shown in Fig. 2(c)) for the different cation columns also suggests that the cation disorder is localized within an area surrounding the 223 SF. This figure shows that far from the "223" SF, the collection of integrated intensity profiles has a higher intensity at the Ba site than at the Y site consistent with little or no cation disorder between the sites. However, the profile changes progressively with closer distance to the SF, where the intensity at the Y site becomes progressively higher than that at Ba sites, indicating the presence of significant

cation disorder. Such localized nature of the cation disorder may explain the absence of T_c degradation for the samples with x values up to 0.15. In this situation a percolative path of zero resistance would exist during the low-current T_c measurement while the self-field J_c would be significantly reduced given the degraded electronic properties of the disordered regions. Defect densities higher than those accommodating roughly all the vortices generated in self field can obviously be a reason for self-field J_c reduction although they can further enhance in-field J_c. However, high J_c over 3 MA/cm^2 was reported for solution processed YBCO films having a density of $YBa_2Cu_4O_y$, "124", SFs of about 68 μm^{-1}, which is higher than the SF density in the x=0.15 sample (~52 μm^{-1}). [23]

The 223 SFs are expected to play the role of strong *ab*-plane correlated pinning centers resulting in an improvement of in-field J_c, particularly for a field parallel to the *ab*-plane, $H \| ab$. The 124-type or $Y_2Ba_4Cu_7O_y$, 247-type SFs have been already demonstrated to act as strong *ab*-plane correlated pinning centers to improve in-field J_c at $H \| ab$. These SFs are also reported to be able to be random pinning centers when the field is away from $H \| ab$.[23-25] Vortices could be pinned by the SFs themselves, or by the partial dislocations that form around the edges of a SF. Figure 3 presents the angular dependence of J_c and normalized J_c with respect to the self-field J_c, J_c/J_c (sf), at 77 K, 1 T. As expected, much higher and sharper J_c peaks at $H \| ab$ are achieved for the samples with x values up to 0.1 due to the presence of 223 SFs in the films, compared to YBCO. For the x=0 and 0.05 samples, J_c values for other field orientations away from $H \| ab$ are also larger than those for pure YBCO films due to their higher self-field J_c compared with pure YBCO. The x=0.15 sample also shows a somewhat sharper J_c peak with a higher ratio of $J_c(H \| ab)/J_c(H \| c)$, but overall J_c values for the entire range of angles are much

smaller due to the smaller self-field J_c of 0.8 MA/cm^2, compared to the pure YBCO film. To investigate flux-pinning properties while excluding the effect caused by the difference in the self-field J_c between the samples, normalized J_c values for the samples are also compared in Fig. 3(b). It is obvious that Sm substitution remarkably enhances the flux-pinning for $H \| ab$. With increasing x, the peak of J_c/J_c (sf) for $H \| ab$ becomes sharper and significantly larger, while the J_c/J_c (sf) values near $H \| c$ are slightly reduced. Stronger *ab*-correlated pinning, resulting in sharper J_c/J_c (sf) peaks for $H \| ab$ with increasing x, is directly correlated to the increased number density of 223 SFs as confirmed by XRD and TEM analyses. Note that the increased cation/oxygen disorder with increasing values of x can also influence the flux-pinning and in-field J_c properties of the samples. However, unlike the *ab*-plane correlated pinning centers created by the 223 SFs, the disorder acts as isotropic-pinning centers and therefore influence flux-pinning equally for all field angles. Such an isotropic pinning enhancement is not observed in these samples.

IV. CONCLUSION

In summary, the effect of Sm substitution on the Ba site as well as on the Y sites on the structural and superconducting properties of YSmBCO films has been investigated. Sm substitution on the Y and Ba sites in YBCO films gives rise to 223 SFs aligned along the *ab*-plane. The stacking fault density was found to increase with increasing amounts of Sm substitution. The sample designed to study only Sm substitution for Y (x=0) resulted in the highest self-field J_c with strongly enhanced flux-pinning for $H \| ab$, which is probably due to forming an optimal density of the 223 SFs. As the value of x was

increased from 0 to 0.15, corresponding to additional Sm substitution on the Ba-sites, the self-field J_c at 77 K gradually decreased. However, the flux-pinning for $H \| ab$ was strongly enhanced by the increased number density of 223 SFs.

Acknowledgments

We would like to thank SuperPower Inc. for providing the Hastelloy substrates with the multilayer configuration of IBAD MgO layer / Homoepitaxial MgO layer / Epitaxial $LaMnO_3$. This research was sponsored by the U.S. DOE Office of Electricity Delivery and Energy Reliability - Advanced Cables and Conductors under contract DE-AC05-00OR22725 with UT-Battelle, LLC managing contractor for Oak Ridge National Laboratory. Research also supported by ORNL's Shared Research Equipment (SHaRE) User Facility, which is sponsored by the Office of Basic Energy Sciences, U.S. Department of Energy. Use of Raman instrumentation at Argonne's Center for Nanoscale Materials was supported by the USDOE, Office of Science, Office of Basic Energy Sciences. The work performed at the Argonne National Laboratory was carried out under contract DE-AC02-06CH11357 between UChicago Argonne, LLC and the U.S. Department of Energy.

References

[1]T. Haugen, P. N. Barnes, R. Wheeler, F. Meisenkothen, and M. Sumption, *Nature* **430**, 867 (2004).

[2]K. Matsumoto, T. Horide, A. Ichinose, S. Horii, , Y. Yoshida, and M. Mukaida, *Jpn. J. Appl. Phys.* **44**, L246 (2005).

[3]J. L. Macmanus-Driscoll, S. R. Foltyn, Q. X. Jia, H. Wang, A. Serquis, L. Civale, B. Maiorov, M. E. Hawley, M. P. Maley, and D. E. Peterson, *Nat. Mater.* **3**, 439 (2004).

[4]A. Goyal, S. Kang, K. J. Leonard, P. M. Martin, A. A. Gapud, M. Varela, M. Paranthaman, A. O. Ijaduola, E. D. Specht, J. R. Thomson, D. K. Christen, S. J. Pennycook, and F. A. List, *Supercond. Sci. Technol.* **18**, 1533 (2005).

[5]S. H. Wee, A. Goyal, Y. L. Zuev, and C. Cantoni, *Supercond. Sci. Technol.* **21**, 092001 (2008).

[6]S. H. Wee, A. Goyal, E. D. Specht, C. Cantoni, Y. L. Zuev, V. Selvamanickam, and S. Cook, *Phys. Rev. B* **81**, 140503(R) (2010).

[7]M Murakami, N Sakai, T Higuchi, and S I Yoo, *Supercond. Sci. Technol.* **9**, 1015 (1996).

[8]S. H. Wee, A. Goyal, P. M. Martin, M. Paranthaman, and L. Heatherly, *Supercond. Sci. Technol*. **19**, L42 (2006).

[9]T. Ozaki, Y. Yoshida, Y. Ichino, Y. Takai, K. Matsumoto, A. Ichinose, S. Horii, and M. Mukaida, *Physica C* **468**, 1615 (2008).

[10]C. Cantoni, D. P. Norton, D. M. Kroeger, M. Paranthaman, D. K. Christen, D. Verebelyi, R. Feenstra, D. F. Lee, and E. D. Specht, *Appl. Phys. Lett.* **74**, 96 (1999).

[11]Q. X. Jia, S. R. Foltyn, P. N. Arendt, H. Wang, J. L. MacManus-Driscoll, Y. Coulter, Y. Li, M. P. Maley, M. Hawley, K. Venkataraman and V. A. Maroni, *Appl. Phys. Lett.* **83**, 1388 (2003).

[12]S. H. Wee, A. Goyal, P. M. Martin and L. Heatherly, *Supercond. Sci. Technol*. **19**, 865 (2006).

[13]Z. S. Peng, J. M. Hao, B. Yin, Z. X. Zhao, Z. Q. Hua, and B. C. Yang, *Physica C* **282-287**, 2103 (1997).

[14]A. R. Devi, V. S. Bai, P. V. Patanjali, R. Pinto, N. H. Kumar, and S. K. Malik, *Supercond. Sci. Technol.* **13**, 935 (2000).

[15]J. L. MacManus-Driscoll, S. R. Foltyn, B. Maiorov, Q. X. Jia, H. Wang, A. Serquis, L. Civale, Y. Lin, M. E. Hawley, M. P. Maley, and D. E. Peterson, *Appl. Phys. Lett.* **86**, 032505 (2005).

[16]T. J. Haugan, T. A. Cambell, N. A. Pierce, M. F. Locke, I. Maartense, and P. N. Barnes, *Supercond. Sci. Technol.* **21**, 025014 (2008).

[17]A. Goyal, S. H. Wee, C. Cantoni, Y. L. Zuev, E. D. Specht, J. Shin, Y. Gao, S. Cook, O. Polat, T. Aytug, K. Kim, J. Sinclair, J. R. Thompson, M. P. Paranthaman, and D. K. Christen: presented at the 2009 Annual Peer Review for the U.S. Superconductivity Program for Electric Systems, August 4-6, 2009, Washington, DC (in preparation for publication).

[18]Certain trade names and company products are mentioned in the text or identified in illustrations in order to adequately specify the experimental procedures and equipment used. In no case does such identification imply recommendation or endorsement by the National Institute of Standards and Technology.

[19]B. D. Cullity and Stuart R. Stock, *Elements of X-ray Diffraction*, 3rd ed. Prentice Hall, Upper Saddle River, NJ, 2001, p. 149.

[20]S. Hendrick sand E. Teller, *Journal of Chemical Physics* **10**, 147 (1942).

[21]C. L. Jia, H. Soltner, B. Kabius, U. Poppe, and K. Urban, *Physica C* **182**, 163-170 (1991).

[22]K. Venkataraman, R. Baurceanu, and V. A. Maroni, *Appl. Spectrosc.* **59**, 639 (2005).

[23]E. D. Specht, A. Goyal, P. M. Martin, X. Li, and M. Rupich, *Appl. Phys. Lett.* **89**, 162510 (2006).

[24]H. Yamasaki, K. Ohki, I. Yamaguchi, M. Sohma, W. Kondo, H. Matsui, T. Manabe, and T. Kumagai, *Supercond. Sci. Technol.* **23**, 105004 (2010).

[25]J. Wang, J. H. Kwon, J. Yoon, H. Wang, T. J. Haugan, F. J. Baca, N. A. Pierce, and P. N. Barnes, *Appl. Phys. Lett.* **92**, 082507 (2008).

Figure captions

Figure 1. X-ray diffraction results for $(Y_{0.667}Sm_{0.333+x})Ba_{2-x}Cu_3O_{7-\delta}$ films with x ranging from 0 - 0.15. (a) θ-2θ scans showing broadening of the (006) peak with increasing x. (b) The width and shift of a series of (00l) reflections. (c) Measured and simulated diffraction patterns for the x = 0 and 0.15 samples. (d) Stacking faults density estimated by Hendricks-Teller model as a function of x.

Figure 2. Cross-section TEM images for YSmBCO samples with (a) x = 0 and (b) x= 0.15. (c) Z-contrast TEM image of a 223 SF which includes extra Y and O layers (designed by arrow). Crystal structures representing YBCO and a 223 SF ($Y_2Ba_2Cu_3O_x$) are illustrated in the right side of the figure. Note that in Y_2O_3, one of the oxygen sites indicated is vacant. Also, the oxygen positions in (c) are speculative since O columns are not distinguishable in the STEM image.

Figure 3. Raman spectra for YSmBCO films with x=0 (red) and x=0.15 (purple) with intensities normalized to the 330 cm^{-1} YBCO mode. These Raman spectra were excited using a 633 nm laser line. They comprise an averaged spectrum obtained by coadding spectra recorded at roughly 30 sample surface locations. The phonon modes at 230 cm^{-1} and 560 cm^{-1} indicate the presence of oxygen disorder and cation disorder, respectively.[22]

Figure 4. Aberration corrected Z-contrast, cross-sectional STEM image for the x=0.15 sample with integrated intensity profiles of atomic columns at the Y and Ba sites.

Figure 5. Angular dependence of J_c and J_c/J_c(sf) at 77 K and 1 T for pure YBCO and $(Y_{0.667}Sm_{0.333+x})Ba_{2-x}Cu_3O_{7-\delta}$ films with x ranging from 0 - 0.15, in a magnetic field applied -30^o to 110^o with respect to the c-axis of the film. For comparison, J_c data for the pure YBCO film with the same thickness are also plotted in the figure (black line).

Table 1. FWHM values of (006) ω- and (113) φ-scans, % cube texture, transport T_c, and J_c at 77 K, self-field for 0.8 μm thick (Y,Sm)BCO films grown on IBAD-MgO templates.

Compositions of the samples	Δω (°)	Δφ (°)	% cube (%)	T_c (K)	J_c (77K,sf) (MA/cm^2)
$YBa_2Cu_3O_{7-\delta}$	1.3	3.2	96	87.7	2.8
$(Y_{0.667}Sm_{0.333})Ba_{2.0}Cu_3O_{7-\delta}$	1.2	2.9	96	88.3	4.05
$(Y_{0.667}Sm_{0.383})Ba_{1.95}Cu_3O_{7-\delta}$	1.1	2.8	95.5	88.4	3.05
$(Y_{0.667}Sm_{0.433})Ba_{1..9}Cu_3O_{7-\delta}$	1.3	2.7	95.1	88.4	2.23
$(Y_{0.667}Sm_{0.483})Ba_{1.85}Cu_3O_{7-\delta}$	1.3	2.7	96	87.4	0.82

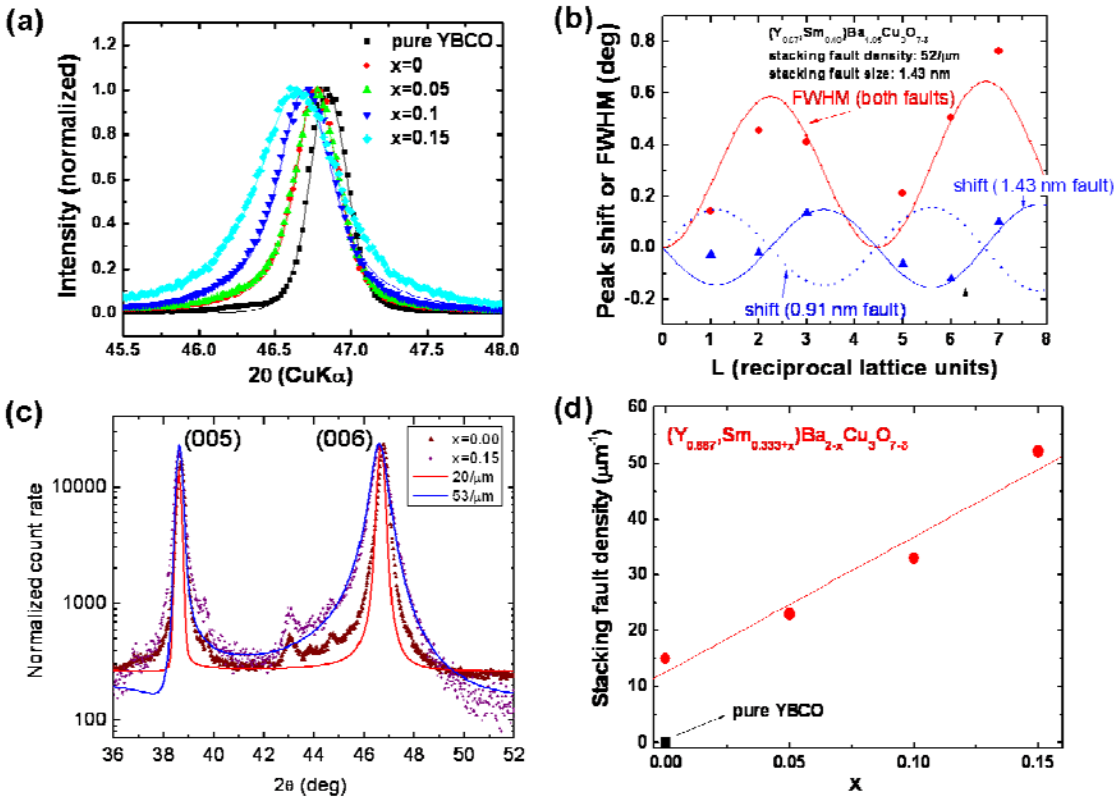
(a)
Intensity (normalized)
2θ (CuKα)
pure YBCO
x=0
x=0.05
x=0.1
x=0.15
(b)
Peak shift or FWHM (deg)
L (reciprocal lattice units)
stacking fault density: 52/μm
stacking fault size: 1.43 nm
FWHM (both faults)
shift (1.43 nm fault)
shift (0.91 nm fault)
(c)
Normalized count rate
2θ (deg)
(005)
(006)
x=0.00
x=0.15
20/μm
53/μm
(d)
Stacking fault density (μm⁻¹)
x
pure YBCO

Figure 1

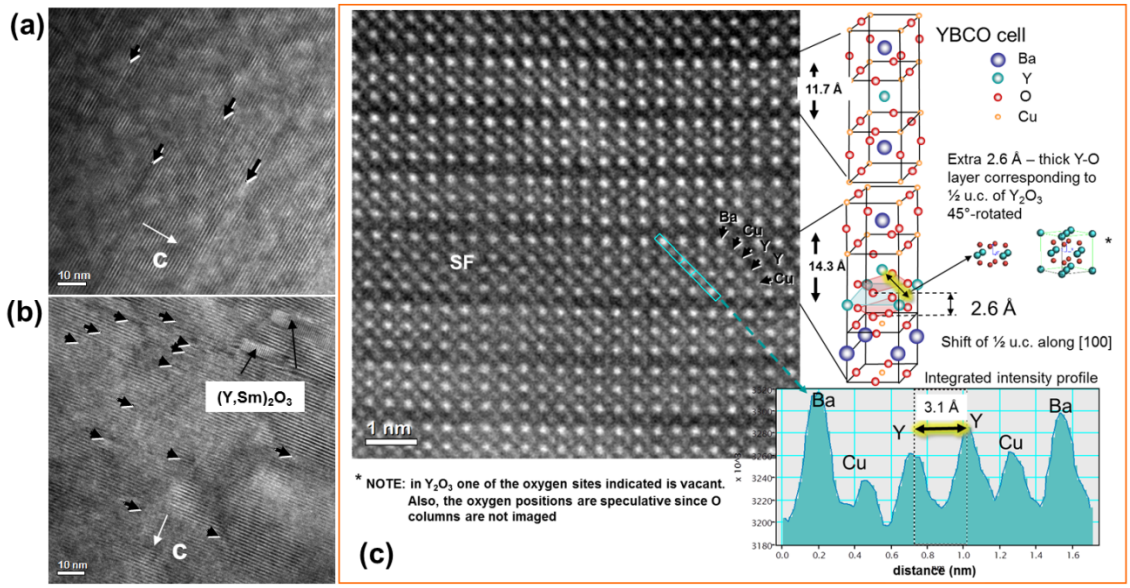
(a)
10 nm
c
(b)
(Y,Sm)2O3
10 nm
c
SF
1 nm
Ba
Cu
Y
Y
Cu
* NOTE: in Y2O3 one of the oxygen sites indicated is vacant. Also, the oxygen positions are speculative since O columns are not imaged
(c)
YBCO cell
Ba
Y
O
Cu
11.7 Å
14.3 Å
Extra 2.6 Å – thick Y-O layer corresponding to ½ u.c. of Y2O3 45°-rotated
2.6 Å
Shift of ½ u.c. along [100]
Integrated intensity profile
Ba
Y
Cu
3.1 Å
Y
Cu
Ba
distance (nm)

Figure 2

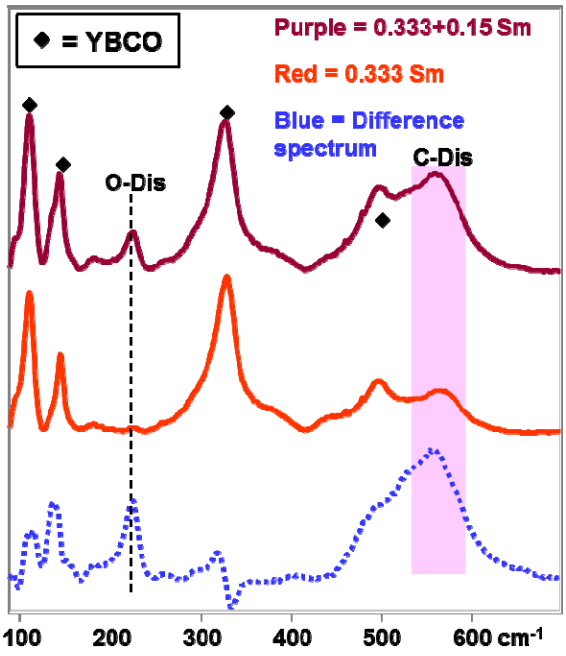
◆ = YBCO
Purple = 0.333+0.15 Sm
Red = 0.333 Sm
Blue = Difference spectrum
O-Dis
C-Dis
100
200
300
400
500
600 cm-1

Figure 3

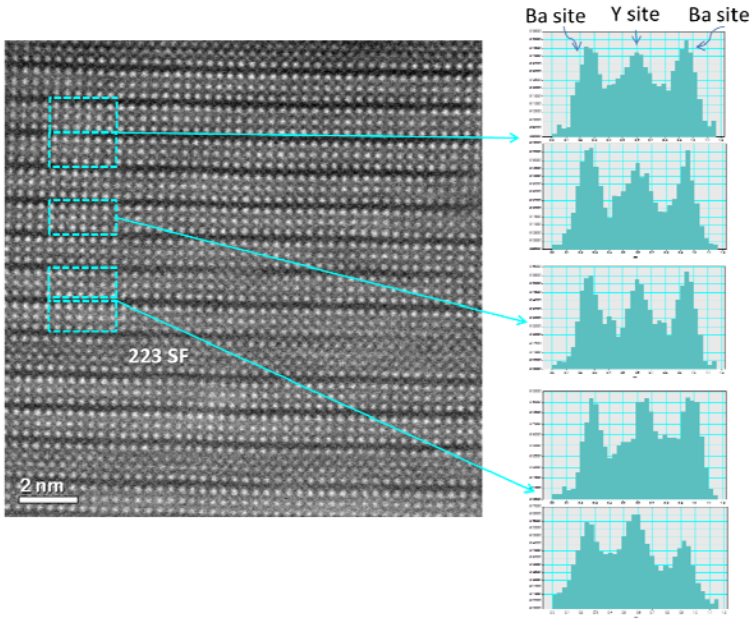

Figure 4

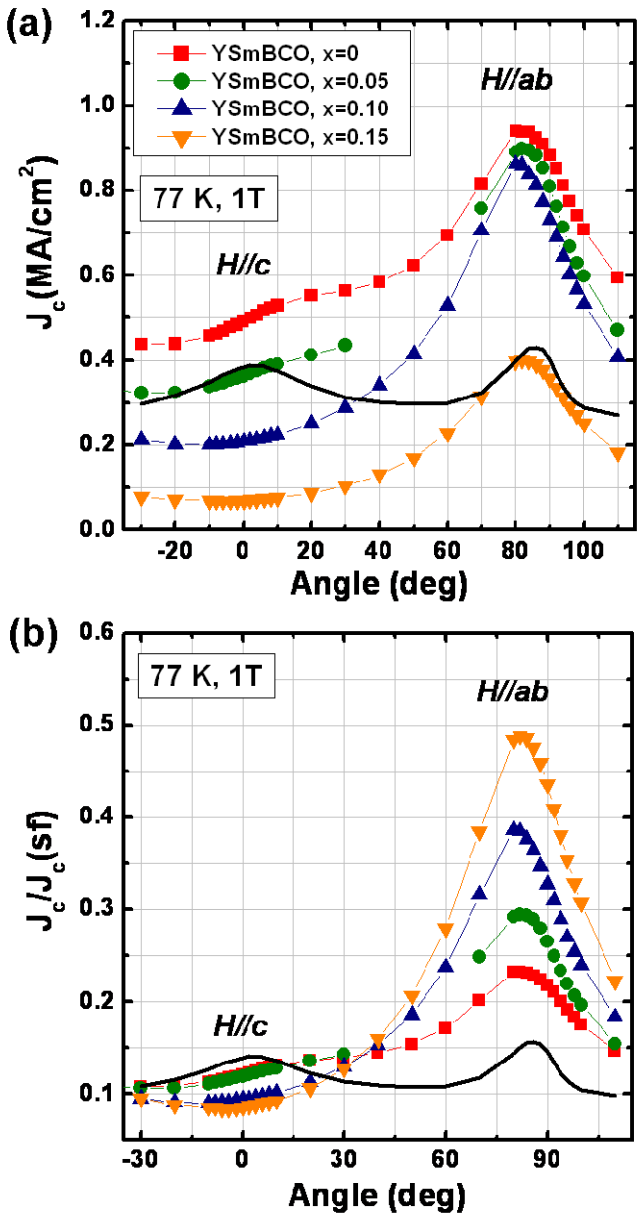
(a)
YSmBCO, x=0
YSmBCO, x=0.05
YSmBCO, x=0.10
YSmBCO, x=0.15
77 K, 1T
H//ab
H//c
J_c (MA/cm^2)
Angle (deg)
(b)
77 K, 1T
H//ab
H//c
J_c /J_c (sf)
Angle (deg)

Figure 5